Machine learning approach reveals heterogeneous responses to FAK and Rho GTPases inhibition on smooth muscle spheroid formation

Kalyanaraman Vaidyanathan[1#], Chuangqi Wang[2#], Yudong Yu[2], Amanda Krajnik[1], Moses Choi[2], Bolun Lin[3], John Kolega[1], Kwonmoo Lee[2*], Yongho Bae[1*]

[1]Department of Pathology and Anatomical Sciences, Jacobs School of Medicine and Biomedical Sciences, University at Buffalo, State University of New York, Buffalo, NY 14203, USA; [2]Departments of Biomedical Engineering and [3]Computer Science, Worcester Polytechnic Institute, Worcester, MA 01609, USA.

[#]These authors contributed equally: Kalyanaraman Vaidyanathan and Moses Choi.

*****Correspondence and requests for materials should be addressed to Y.B. (yonghoba@buffalo.edu) and K.L. (klee@wpi.edu)

ABSTRACT

Hyper proliferation of vascular smooth muscle cells (VSMCs) contributes to neointima formation in atherosclerosis and the response to vascular injury. Understanding how to control VSMC proliferation would advance the effort to treat vascular disease. Drug responses are often different among patients with the same vascular disease condition, making it difficult to cater patient-specific treatments (existence of heterogeneity). Thus, we examined variations in response to drug treatments using VSMC spheroids that mimic vascular disease condition in vivo. FAK and its downstream Rho GTPases (Rac, Rho, and Cdc42) control cell-cell contact and play a key role in vascular pathology. Here, we tested the importance of FAK and Rho GTPases in spheroid formation. VSMC spheroids were made using a hanging-drop method with either inhibitors or vehicle control. Changes in morphology were used as a key indicator of spheroid response to drug treatment. A machine learning (ML) image segmentation (VGG16-U-net) was used to segment the spheroid images. After the morphological features were extracted from the segmented images, a two-level cluster framework was used to cluster VSMC spheroids into different morphologies. We found that FAK and Rho GTPases are required for normal spheroid formation. Next, we analyzed the various morphologies of disrupted spheroids resulting from drug treatment using our ML pipeline. The first-level clustering analysis showed the presence of 4 clusters of spheroids with rounded and disrupted morphologies. The subsequent second-level clustering analysis identified the presence of four distinct morphological clusters among these disrupted spheroids, and they exhibited differential responses to FAK and Rho GTPases inhibition. Particularly, we found FAK and Rho specific morphological phenotypes, thus suggesting that there may be two distinct pathways governing VSMC spheroid formation. Collectively, we revealed there are significant heterogeneities in the drug responses of spheroid formation, which were overlooked in previous analyses. This is our first step towards developing the ML-based method that can be used to assess the effects of different drugs on the VSMC spheroid model for better characterization of pathologic progression of vascular disease.

INTRODUCTION

Vascular smooth muscle cell (VSMC) proliferation, which is regulated by the cell cycle machinery, is critical to many biological processes in vascular biology and disease. Uncontrolled VSMC proliferation is one of the main features of atherosclerosis and vascular restenosis, which contributes to vascular hyperplasia, neointima formation, and vessel thickening and hardening. Neointima formation in atherosclerosis and the response to vascular injury can reduce blood flow by partially occluding the vessel (Fig. 1)[1]. Though VSMC proliferation occurs during normal vascular development and repair of vascular injury, pathologies arise when VSMCs fail to cease proliferation once vascular remodeling has been completed, as occurs in neointima formation and atherosclerotic stenosis[2]. Endovascular surgical procedures including balloon angioplasty are used to open the occluded vessel and restore blood flow. However, a major consequence of this technique is the reintroduction of neointima hyperplasia and thus restenosis of the blood vessel (vascular injury). Although, the introduction of stents coated with anti-proliferative chemicals has perhaps made the most meaningful clinical impact in recent years on reducing neointimal thickening. The highly toxic, nonspecific chemical agents used in these settings also increase the risk of thrombotic cardiovascular events, by interrupting the healing response around the stents, further complicating the treatment of neointima hyperplasia[3]. Thus, we have focused on further exploring the direct inhibition of specific molecular mediators of VSMC function responsible for neointima formation *in vivo*, which may be used therapeutically to prevent neointima formation.

To study the formation of the neointima, we used a 3D spheroid-based suspension culture method. Note that the spheroid model is a commonly used technique in investigating tumor formation, which results from hyper-proliferation, increased cell-cell adhesions, and increased extracellular matrix (ECM) production and deposition. In our study, we used VSMCs, a major cellular component of neointimal lesions, and developed a 3D VSMC spheroid system that mimics restenosis-like neointima formation. VSMCs are held together in the neointima and in the 3D spheroid by cell-cell adhesion associated with proteins like cadherin[4-6]. VSMCs forming the

neointima on the vessel wall and spheroids in vitro function due to the interactions among cells, between cells, and the surrounding ECM secreted by the cells. The involvement of extracellular matrix (ECM) in the regulation of proliferation and the phenotypic modulation of VSMCs has been a focus of research on neointima formation after vascular injury. The ECM plays an important role in neointimal thickening because it contributes between 60% and 80% of mass to the neointimal formation[7]. ECM modifications are sensed by integrin, a transmembrane protein that facilitates cell-ECM adhesions and mechanical signal transduction[8]. Integrins cluster at the cell-ECM interaction site and increase the overall strength of the cell attachments to the surface of ECM. The signal transduction by integrin begins when it binds to ECM proteins and induces activation of many proteins attached to them in the cytosolic domain within the cells. Focal adhesion kinase (FAK) is a non-receptor tyrosine kinase and one of the major focal adhesion proteins in cells activated by ECM-integrin interactions[9]. Among other functions regulated by FAK, in our study cell-cell adhesions are of major focus in neointima formation. The integrity of the spheroid architecture and the hyperplasia plaque is maintained by cadherins that are responsible for cell-cell adhesion and increased proliferation of VSMCs. N-cadherin is shown to be upregulated in VSMCs as a result of vascular injury[10]. N-cadherin has been shown to affect cell-cell adhesions as well as cell migration, proliferation and apoptosis[11-13].

FAK regulates cellular functions through various downstream small G-proteins including Rac, Rho and Cdc42. These small G-proteins act as dynamic molecular switches within the cell, alternating between a GDP-bound inactive state, and a GTP-bound active state. Rho activity has been shown to promote stress fiber formation, focal adhesion formation, and cell contractility. Rho-associated protein kinase (ROCK)[14], a downstream target of Rho, is essential for integrin-mediated cell-cell adhesions and is involved in myosin light chain phosphorylation, which leads to the formation of focal adhesions. Rho/ROCK inhibitors have been used in animal models of vascular injury to prevent restenosis[15]. FAK regulates Rho activity through SFKs (Src family of tyrosine kinase), and can potentially regulate cell-cell adhesions and spheroid formation through

Rho[16]. Rac regulates actin polymerization, membrane ruffling, lamellipodia extension, and cadherin-based cell-cell adhesion. FAK is the upstream regulator of Rac and could influences spheroid formation potentially through Rac mediated cell-cell adhesion. Finally, activation of Cdc42 is necessary for actin polymerization and tension development in tracheal smooth muscle tissues[17]. An increase in Cdc42 activation has been also shown to increase actin polymerization in the cell-cell adhesion junctions. Cdc42 is known to regulate the β-catenin-cadherin-mediated cell-cell adhesion. Currently, there are no described scientific reports specifically associated with Cdc42 and blood vessel formation or function, which makes it a potential new target to study with respect to spheroid and neointima formation[17-20].

Automated image segmentation techniques have been focused on analyzing the shapes (morphologies) of spheroids to better understand their biological significance. We studied the morphology of 3D VSMC spheroids and its biological significance in response to drug treatment. The first step in studying the shape of spheroids is to identify the outline or boundary of the spheroids. Edge detection or boundary analysis is an image processing technique for finding the boundaries of objects within images. Edge detection works by detecting discontinuities in brightness. The most common and typical segmentation methods like intensity thresholding fail to analyze the boundary parameters using phase contrast or bright-field images. These segmentation methods are required to use fluorescent images to precisely analyze the boundaries of spheroids as certain boundary features have a similar intensity to the background field of the image. Recent developments in supervised image segmentation techniques have made segmenting complex cell shapes possible with higher precision without fluorescent labeling and solved the issue of boundary analysis by learning more boundary parameters. U-Net, VGG16, DeepEdge, DeepCountour are available natural image segmentation methods proposed for a machine learning (ML)-based cell boundary determination technique that requires minimal training data to learn boundary parameters. These techniques are human-assisted, semi-supervised learning techniques that use manual segmentation to learn pixels on the boundaries

of objects for better segmentation of object boundaries.

The U-Net convolutional neural network architecture is commonly used for the precise segmentation of images. The U-Net architecture works with very few training images and could learn boundary parameters to identify cellular boundaries with little human supervision. In total, the network has 23 convolutional layers, hence more boundary features could be studied in relatively lesser time [21]. The VGG16 convolutional neural network model is designed for large-scale image recognition with greater depth. The architecture is shown to achieve excellent performance even when used as a part of a relatively simple pipeline and requires minimum training data [22]. We used the combination of the two high-performance segmentation algorithms to segment the spheroid images as previous literature showed that combining VGG-16 with U-Net is less prone to errors in segmentation compared to solely using U-Net [23]

In this study, we examined the importance of FAK and downstream small G-protein (Rac, Rho, and Cdc42) signaling in 3D VSMC spheroid formation. We proposed FAK-Rac, FAK-Rho and FAK-Cdc42 mediated pathways for VSMC spheroid formation and maintenance of spheroid structural integrity through N-cadherin mediated cell-cell adhesion. We found that FAK and downstream small G-proteins' inhibition disrupted VSMC spheroid morphology, indicating that FAK, Rac, Rho and Cdc42 are required for normal spheroid formation. Interestingly, inhibition of FAK, Rac, and Rho, but not Cdc42, caused a significant reduction in N-cadherin expression. Furthermore, we computationally represented the variations in drug responses amongst VSMC spheroids. Fascinatingly, the clustering analysis showed the presence of morphological subpopulations amongst the VSMC spheroids that arise due to treatment with the drugs. The morphological subpopulations seen in the cluster signal the presence of possible biological cues that could be targeted for developing pharmacological treatments which are targeted to a particular shape/morphology.

RESULTS

FAK inhibition disrupts spheroid formation

FAK is a key signaling molecule in the regulation of vascular cell-cell contact formation, vascular development and network stability[24,25]. To test the importance of FAK activity in 3D VSMC spheroid formation that mimic neointima formation on the vessel wall *in vivo*, we cultured human VSMCs (hVSMCs; Fig. 3A and 3B) and mouse VSMCs (mVSMCs; Fig. 3C and 3D) to form vascular smooth muscle spheroids in the presence of either PF573228 (a pharmacological inhibitor of FAK) or DMSO (a vehicle control); note that FAK activity (pFAK, which is the active form of FAK) in both hVSMCs (Fig. 3A) and mVSMCs (Fig. 3C) was reduced about 70-80% by 10 μM PF573228. The images were acquired at 24 hours due to the doubling time of VSMCs being between 32-48 hours, subsequently eliminating the effect of cell proliferation. Microscopy images showed that FAK inhibition significantly disrupted spheroid formation and morphology of both hVSMC (Fig. 3B) and mVSMC (Fig. 3D) as compared to spheroids treated with DMSO. Interestingly, both control and FAK-inhibited spheroids were varied formation/morphologies in both hVSMC (Fig. 4A, panels 1 to 6) and mVSMC spheroids (Fig. 4B, panels 1 to 6). The experiments were repeated for n=7 biological repeats for hVSMC spheroids and n=12 for mVSMC spheroids. Overall, FAK is required for normal VSMC spheroid formation; however, the effect of FAK inhibition on spheroid disruption is heterogeneous.

Rac, Rho, and Cdc42 are essential for VSMC spheroid formation

Rac, Rho and Cdc42, major downstream targets of FAK signaling, have been implicated in the regulation of cell morphology and cell-cell adhesion [24,26,27]. More importantly, Rac, Rho, and Cdc42 are essential for VSMC proliferation, vascular remodeling, and neointima formation. We therefore asked if FAK inhibition disrupts VSMC spheroid formation through Rac, Rho, and/or Cdc42. We cultured hVSMCs in the presence of inhibitors of 5-20 μM EHT1864 (a Rac inhibitor), 5-20 μM Rhosin (a Rho inhibitor), or 5-10 μM ML141 (a Cdc42 inhibitor), or vehicle control

(DMSO). Spheroids were imaged after 24 hours of incubation using an upright microscope. Spheroids treated with 5 and 10 μM EHT1864 (Fig. 5A, rows 2 and 3) and 5 and 10 μM Rhosin (Fig. 5B, rows 2 and 3) had the minimal effect in the formation of VSMC spheroids. Whereas, VSMC spheroid formation was significantly disrupted with higher dose (20 μM) in EHT1864 (Fig. 5A, row 4) and Rhosin (Fig. 5B, row 4), and with 5-10 μM ML141 (Fig. 5C, rows 2 and 3) as compared to DMSO-treated VSMC spheroids (Fig. 5A-C, rows 1). We conclude that the small G-proteins Rac, Rho, and Cdc42 are required in VSMC spheroid formation. Interestingly, it was observed that the disruption patterns of spheroid formation were near homogenous with both 5 and 10 μM of ML 141 treatment. This observation shows that the response to inhibition of Cdc42 is completely different than that of Rac- and Rho-mediated disruption. This observation is of high importance because Rac, Rho and Cdc42 have a common upstream regulator in FAK.

FAK, Rac, and Rho inhibition disrupts spheroid formation through N-cadherin

Based on the results shown in figures 3-5, disruption of VSMC spheroid formation may relate to weakening of cell-cell adherens junctions, a site for cadherin-dependent cell adhesion, leading to a reduction in VSMC accumulation. N-cadherin is a major cadherin and a downstream molecule of FAK, Rac, Rho and Cdc42 in VSMCs[28,29]. Mui *et al.,* recently showed that N-cadherin was upregulated in the neointima and underlying tunica media of mouse injured arteries[12]. These injury VSMC-specific responses, such as proliferation and neointimal formation, were significantly decreased in the absence of N-cadherin in VSMCs[12]. This study suggested along with our data showing FAK inhibition to be important in VSMC spheroid disruption that N-cadherin could be a potential downstream regulator of FAK-mediated VSMC spheroid formation. To assess N-cadherin that mediates FAK, Rac, Rho, and/or Cdc42 signals into VSMC spheroid formation, we examined the total levels of N-cadherin induction by immunoblotting. A significant reduction in N-cadherin expression was observed with FAK inhibition as compared to control spheroids (Fig. 6A). In spheroids treated with 20 μM EHT1864 and 20 μM Rhosin, modest reduction of N-cadherin

expression was observed, respectively (Fig. 6B and 6C). Interestingly, however, inhibition of Cdc42 with ML141 did not affect N-cadherin induction (Fig. 6D). Additionally, these results indicate that FAK-Rac and FAK-Rho signaling pathways selectively regulate the formation of VSMC spheroid through N-cadherin.

Developing a VGG16-U-Net semantic segmentation to study VSMC spheroid formation

The data presented in figures 4 and 5 showed that both control and FAK, Rac, Rho or Cdc42-inhibited spheroids were widely varied in morphology and formation. Thus, we further examined changes in spheroid morphology and formation using a ML image segmentation, followed by k-means clustering analysis to visualize the presence of morphological subpopulations resulting from drug treatments.

First, spheroid boundaries were manually drawn on a subset of images using Pixel Annotation Tool (Fig. 7A), and these annotated images were then used to train the VGG16-U-Net. When provided with new images outside the training set, the trained algorithm identified boundaries with 95% accuracy. This learning rate was plotted as dice coefficient vs. training loss and was observed that loss was reduced with increasing epoch (training cycle) number (Fig. 7C). The test images were provided to the evaluation algorithm and the output of the raw image masked over by binary images was developed (Fig. 7B, middle panel). The images visually provided confirmation that the algorithm was trained to the best efficiency. Lastly, the morphological features of the spheroid images were extracted by the trained VGG16-U-Net segmentation architecture and the z-score was normalized. Plotting the values in the Umap plot showed the presence of variation in spheroid morphology and formation in response to drug treatment.

Morphological features identify the variations in spheroid formation in responses to drug treatment.

Four morphological features were selected relating to the roundness of the object. These four features were plotted as an Umap plot, a dimensionality reduction technique (Fig. 8)[30,31]. The data points on the plot represent morphological features extracted from spheroid images treated with different drug treatments (FAK, Rac, Rho, and Cdc42 inhibitor) or vehicle control (DMSO). The plot in figure 8 showed the data points corresponding to each drug or DMSO treatment group scattered through the plot area. This plot indicated the presence of morphological variations in drug response. Further, k-means clustering was used to cluster the points into various morphological clusters.

Coarse clustering analysis defines the presence of morphological subpopulations

The Umap plots were obtained by plotting feature vectors from spheroid images. A community detection technique was used to determine the number of clusters for k-means clustering. The value for the number of nearest samples with the highest silhouette value was used as the cluster number (Fig. 9A). The resulting plots showed the presence of 4 distinct clusters with varied fractions of DMSO and drug-treated spheroid groups (Fig. 9B). The k value of 4 was picked based on the silhouette values for the number of nearest samples between 2 and 200. A cluster value of 4 showed the least overlap between clusters and mostly positive silhouette values when the silhouette map was plotted (Fig. 9C). The distribution of spheroid morphologies in each cluster was represented as a proportion of data points in each cluster (Fig. 10A). The cluster number was plotted along the x-axis and the proportions are represented along the y-axis. It was observed that hVSMC spheroids with DMSO were mostly present in cluster 1 (about 65% of the total DMSO, Fig 10B). PF573228 treated hVSMC spheroids were present in clusters 2 and 4 about 50% and 40% of the total, respectively. Spheroids in clusters 2 and 4 were mostly non-circular or displayed disrupted morphology. Cluster 1 had the highest proportion of 5 μM and 10 μM EHT1864 (about 70% of total) and 5 μM and 10 μM Rhosin (60% of the total). Cluster 3 had over 80% of the total ML141 treated spheroids (Fig. 10B). When spheroid images were mapped to the clusters, the

spheroids in clusters 1 and 3 showed rounded morphology. The spheroids in clusters 2 and 4 represented more of a disrupted or dispersed morphology (Fig. 11).

Fine tuning analysis shows the presence of four distinct clusters with disrupted morphology

To get finer clusters of more disrupted/dispersed spheroids, the spheroids in the clusters 2 and 4 were subjected to further morphological feature extraction. DMSO treated spheroids were manually removed, to take into account only the disrupted morphology. The 15 features were specially selected to represent the morphologies of disrupted spheroids as referred in chapter 3.4.7 and Fig. 2. The morphological features extracted from the spheroids from clusters 2 and 4 were plotted on Umap (Fig. 12) and k-means clustering analysis was performed. Community detection technique[32] was used to determine the number of clusters. The value for the number of nearest samples with the highest silhouette value was used as the cluster number. The resulting plots showed the presence of 4 distinct clusters with varied fractions of DMSO and drug-treated spheroid groups (Fig 13A). The k value of 4 was picked based on the silhouette values for the number of nearest samples between 2 and 200. Cluster value 4 showed the least overlap between clusters and mostly positive silhouette values when the silhouette map was plotted (Fig. 13B). The four clusters were plotted and proportionality plots were drawn (Fig. 14A). The cluster distribution showed that cluster 1 had the maximum number of FAK inhibited spheroids and cluster 3 had the maximum number of Rho inhibited spheroids. Rac inhibited spheroids were distributed between all four clusters (Fig 14B). Due to the coarse clustering analysis, Cdc42 spheroids were mostly distributed in clusters 1 and 3 and others were manually removed. Hence, they were not observed in the fine clustering.

The data points from the clusters were used to identify the spheroid images from which they were obtained. Once the spheroids were identified the images were then organized based on the morphological subpopulation that was observed post clustering and two representative

images were displayed on the cluster Umap plot (Fig. 15A). Clusters 1 and 2 that contained the maximum FAK treated group spheroids showed the least disruption in spheroid formation, and clusters 3 and 4 showed the greatest disruption in spheroid formation (Fig. 15B).

The data obtained from both coarse clustering and fine-tuning clustering analyses were then combined to display the distributions of VSMC spheroids treated with inhibitors of FAK, Rac, Rho or Cdc42, or DMSO. The proportionality plot for six clusters (clusters 1 and 3 from coarse clustering Figure 10B and clusters 1-4 from fine clustering figure 114B) was plotted. The resulting proportionality plot and the total data set of spheroid images were clustered into 6 (2 rounded and 4 disrupted) different morphologies (Fig. 16).

DISCUSSION

VSMC proliferation is a key contributor to neointima formation in vascular pathology. Several studies have demonstrated that FAK and its downstream small G-proteins (Rac, Rho, and Cdc42) are key regulators of VSMC proliferation, mostly by using a 2D cell culture system [12,33]. Yet, the role of FAK and small G1-proteins on the proliferation of VSMCs in a 3D model has not been well explored. In this study, we examined the role of FAK and downstream small G1-proteins in regulating 3D VSMC spheroid formation, a model of neointima formation. We found that FAK, Rac, and Rho but not Cdc42 were found to disrupt spheroid formation and interestingly, we also identified the presence of morphological subpopulations in response to drug treatments using a VGG16-U-net semantic segmentation and K-means clustering analysis.

VSMC spheroids as a model system for neointima formation

Neointimal plaques are aggregations of proliferating and adherent VSMCs, which are a shared property of cell spheroids. Thus, the suspension based culture method can be used as a natural *in vitro* model for studying neointima formation through assessment of spheroid disruption patterns after treatment of drugs that block proposed pathways that favor neointima formation. *In*

vitro cell aggregates form a complex 3D architecture and intensive cell-cell contacts. These contacts are mandatory for the normal function of most tissues. VSMCs are held together in the neointima generated and in the 3D spheroid by cell-cell adhesion associated proteins like cadherins. VSMCs in the neointima, like spheroids, sustain functions due to cellular interactions, and internalized signals from the surrounding ECM secreted and maintained by the cells.

Neointima *in vivo* develops with damage to the arterial wall, followed by platelet aggregation at the site of injury, recruitment of inflammatory cells, proliferation and migration of VSMCs, and ECM deposition. While this process resolves smaller insults to the arterial wall, its persistence in chronic injury becomes pathological, creating the need to resolve these changes This collective process in vessel wall insult resolution is not accounted for in my VSMC spheroid model as it only comprises that of neointima formation-specific VSMC functions, and a major limitation. However, my focuses on disrupting neointima formation may lead to treatments that prevent the narrowing of blood vessels and reduces blood flow. Also, given the rapid workflow of forming spheroids with drug treatments and imaging those using bright field microscopy, this model is convenient as a high-throughput drug screening technique and may become a powerful tool in the study of neointima biology.

In our VSMC spheroid 3D model, we used a modest 2000 cells per spheroid that give a small overall spheroid size being roughly a few hundred microns, which drastically reduces necrotic damage to its core. Other spheroid culture models require a large cell count and the use of a matrigel matrix to aid spheroid growth[34]. Moreover, the external matrigel could significantly affect Spheroidization, making my model more functional along with being more cost-effective.

FAK is required for VSMC spheroid formation

FAK inhibition (using PF 573228) leads to marked disruption in spheroid formation. In-kind, FAK inhibition results in a reduction of cell-cell junctional proteins such as N-cadherin leading to loss of cell-cell adhesions. A significant reduction in N-cadherin upon FAK inhibition suggests that FAK

regulates spheroid formation by regulating cell-cell adhesion. Integrin-mediated FAK activation is required for forming and maintaining cell-cell adhesions[12,27]. Laszlo et al. reported that FAK inhibition reduces spheroid numbers without an increase in spheroid size in mesothelioma, supporting that FAK is required for spheroid formation[27]. Hajime Yano et al. reported that integrin-mediated FAK downstream effectors are necessary for maintaining cell-cell adhesions[35]. The results observed suggest that FAK regulates spheroid formation potentially through N-cadherin. Further experimentation such as immunofluorescence or N-cadherin knockout and recovery experiments in spheroids are necessary to confirm that FAK regulation of N-cadherin reduces spheroid formation.

A Potential mechanism for FAK regulation on VSMC spheroid formation

Furthermore, my study explores the role of FAK downstream small G-proteins (Rac, Rho and Cdc42) in spheroid formation to determine exactly how of spheroid formation is disrupted upon FAK inhibition. Integrin-mediated FAK regulates cell functions through its downstream small G-proteins. Active FAK binds to Src and this complex stimulates Rac1 activity through the recruitment and phosphorylation of p130Cas. The GTP bound active state of these proteins have an impact on multiple biological processes including cell-cell contacts as they control actin polymerization and cytoskeletal reorganization. Rac, Rho, and Cdc42 influence cadherin based cell-cell adhesions by regulating β-catenin, which regulates cadherin-mediated cell-cell adhesion. Our observed result of a spheroid disruption using FAK inhibitor could potentially be regulated through downstream proteins Rac, Rho, and Cdc42, therefore that could have resulted in a reduction in adhesion proteins leading to loss of cell-cell contacts.

We found that spheroid disruption occurs when treated with a Rac inhibitor (EHT1864) at 20uM concentration. A study using mesenchymal stem cells showed that N-cadherin mediated cell-cell adhesion and expression is modulated by Rac signaling[36]. *Bae et al.,* (2014) showed that there is an increase in tissue stiffness after a fine-wire vascular injury to the intimal layer. VSMCs

that upregulate Rac also exhibit downstream N-Cadherin activation in response to vascular injury and increased stiffness[12]. In my study, the disruption of spheroids could due to cell-cell adhesion loss, given Rac's role in promoting cell adhesion[35]. Collectively, FAK is the upstream regulator of Rac and N-cadherin expression is reduced in the absence of activation of the prior two, we suggest a potential signaling pathway where FAK influences spheroid formation through Rac mediated cell-cell adhesion.

Rhosin (Rho inhibitor), at 20 μM concentration, also disrupted spheroid formation and led to a significant reduction in N-cadherin expression. Activation of Rho in VSMCs has been shown to affect cytoskeletal remodeling by both inducing actin stress fiber depolymerization and inhibiting the myosin light chain phosphatase, which are under Rho control. The same study found that cadherin dependent cell-cell contacts destabilized when endogenous Rho was inhibited[37]. FAK regulates Rho activity through SFKs (Src family of tyrosine kinase) and now, we have shown that FAK can potentially regulate cell-cell adhesions and spheroid formation through Rho[16].

Unlike Rac and Rho, we found that Cdc42 inhibition using ML141 resulted in disruption of spheroid formation with no significant changes in N-cadherin levels. The direct connection of Cdc42 to VSMC mediated hyperplasia and NI formation remains unexplored. Cdc42 is known to regulate attachment of actin fibers to the sites of cell-cell adhesion, inhibition of Cdc42 could have resulted in a reduction in levels of adherent junction proteins (e.g., occludin, desmosomes) other than N-cadherin[38] which might have resulted in disruption of the spheroids.

Since both Rac and Rho both are downstream FAK effectors and their loss of activity leads to a reduction in N-cadherin expression, FAK can potentially regulate spheroid formation through both Rac and Rho mediated pathways.

Spheroid morphologies

A salient observation presented in my study is the presence of various heterogeneous morphologies of disrupted spheroids resulting from the treatment with FAK, Rho, Rac, and cdc42

of inhibitors. The first four morphological feature vectors extracted (using VGG16-U-net semantic segmentation) were used to cluster spheroid morphologies using k-means clustering analysis. This resulted in four clusters of morphologies solely based on the roundness of the spheroids. Further, fine-tuning clustering analysis on initial clusters showed the presence of morphological subpopulations as a result of drug treatments.

The spheroids from clusters 2 and 4, in the first level of clustering, showed non-circular morphology. They showed more of a disrupted morphology. Hence, fine-tuning the cluster analysis for the spheroids in clusters 2 and 4 would reveal the presence of morphological subpopulations amongst disrupted spheroids. At this point, DMSO spheroids were manually removed to avoid mis-clustering. The remaining spheroids from the drug-treated groups were subjected to feature extractions with fifteen features. These features were focused on studying the morphological patterns of the disrupted spheroids. Fine-tuning clustering analysis revealed the presence of four more morphologically distinct clusters. These spheroids showed the presence of different disrupted morphologies and could be grouped into smaller clusters.

The VGG16-U-net semantic segmentation is a novel combination of architecture developed by Chuangqi et al., (2019), it combines the use of U-Net and VGG-16 based image segmentation algorithms[23]. Unlike a simple ML algorithm that uses binary thresholding to study cell structures, deep learning is designed to look at more in-depth pixel information to study cellular structures. In comparison to U-net, the VGG16-U-net uses a smaller training set and attained close to zero training loss (errors in identifying the parameters) with lower epoch number (number of cycles needed to train an algorithm training) and was able to achieve higher validation and precision in boundary determination.

The establishment of these morphological subpopulations as a result of drug treatments was observed in other literature previously published. For instance, Michele Zanoni (2016) reported the presence of morphological heterogeneity amongst tumor spheroids and clustered into various morphological shapes of spheroids that could be classified into the proliferative

ability[39]. With my data, exploring the biological significance of these morphological clusters could result in understanding the morphology to the biological relationship. In vascular neointima formation, Joel Chappell *et al.,* reported that only a small population of vascular smooth muscle cells underlying the site of injury is actively involved in hyperplasia resulting in the neointima formation. Neointima formation was induced in mouse arteries, and upon staining for smooth muscle actin after 28 days. It showed that only a subpopulation of cells underwent the characteristic phenotypic switch and contributed to the NI formation[40]. Moreover, a recent study on pancreatic cancer spheroids by Jennifer Laurent *et al.,* reported that the cells in the multicellular tumor spheroids showed varying effects in response to anti-proliferative drugs. This variation in results was attributed to the size of the spheroids and the packing of cells in the spheroids[41]. Michele Zanoni *et al.* reported that the shape and volume of spheroids are responsible for the variations in response to drug treatment irrespective of cell types. The work also explores an automated shape analyzer to classify tumor spheroid based on shape. When they compared the viability of spheroids homogeneous in volume but varying in shape, a statistically significant difference was noted because of the irregular morphology of the 3D colonies. The number of cells exposed to high levels of nutrients, oxygen dictated the response of the irregularly shaped spheroids[39].

CONCLUSION

This study tested the importance of FAK and its downstream small G-proteins (Rac, Rho, and Cdc42) in 3D VSMC spheroid formation and revealed the presence of various morphological subpopulations among spheroids in response to pharmacologic manipulations. FAK, Rac and Rho inhibition significantly impairs VSMC spheroid formation through downregulation of N-cadherin indicating that signaling pathways linking FAK-Rac-N-cadherin or FAK-Rho-N-cadherin are required for VSMC spheroid formation.

The VGG16-U-Net algorithm was used for segmenting. The plots between vehicle control

and drug-treated groups showed distinct separation amongst clusters of various groups. The clusters developed using k-means clustering analysis showed the presence of various morphologies amongst the DMSO and drug-treated groups, upon coarse clustering. When fine-tuned with just the clusters showing disrupted morphologies, four further clusters were revealed showing distinct subpopulations of morphologies among the disrupted spheroids. These clusters upon further study could give rise to a biological significance. The biological significance of this morphology will be a stepping-stone to identify potential pharmaceutical drug targets. This method of using morphological features to show the variations in responses amongst spheroids resulted in six different morphologies resulting from drug treatments.

Results shown in our study suggest that there are significant morphological subpopulations in 3D VSMC spheroid formation in response to drug administration, which have been overlooked in previous analyses and studies. Overall, this is the first step towards developing an automated ML approach for quickly and precisely analyzing the various effects of drugs on neointima formation and identifying subpopulations among drug-treated vascular spheroids. Our study will allow for a better understanding of vascular biology and characterizing the pathophysiology of vascular diseases like atherosclerosis and vascular injury.

METHODS

Cell culture and drug treatment

Primary human vascular smooth muscle cells (hVSMCs, ATCC) and mouse VSMCs (mVSMCs, Cell Biologics) were cultured as previously described [42,43]. hVSMCs were used at passages 4-10. mVSMCs were used at passages 2-5. For serum starvation (to synchronize cells), near confluent VSMCs were incubated for 48 hours in serum-free media containing 1 mg/ml heat-inactivated, fatty-acid free bovine serum albumin (BSA; Tocris).

For FAK, Rac, Rho, and Cdc42 pharmacologic inhibitor experiments, cells in suspension culture were treated with 10 µM FAK specific inhibitor PF573228 (Sigma), 5-20 µM Rac specific

inhibitor EHT1864 (Tocris), 5-20 µM Rho specific inhibitor Rhosin (Tocris), or 5-10 µM Cdc42 specific inhibitor ML 141 (Tocris) in Dimethyl sulfoxide (DMSO) for selected times up to 24 hours.

Generation of VSMC spheroids

VSMC spheroids were formed using hanging drop culture [44]. Serum-starved cells were trypsinized, centrifuged, and resuspended in fresh high-glucose (4.5g/L) DMEM containing 10% fetal bovine serum (FBS). Total cell numbers were counted with a haemocytometer. Cell suspension was diluted to have 2000 cells per 20 µL high-glucose DMEM with 10% FBS and treated with either DMSO (vehicle control), 10 µM PF573228, 5-20 µM EHT1864, 5-20 µM Rhosin or 5-10 µM ML141 prior to plating. 20 µM of ML141 was reported to be highly toxic to the cells, and was not used. Approximately 20 to 30 cell-suspension droplets were dispensed on hydrophobic surface of the lid of a 100-mm tissue culture dish. Note that the drops are seeded sufficiently apart to avoid the mixture of each adjacent drop. To prevent evaporation of the drops, a water reservoir (hydration chamber) was made by adding 8 ml of sterile water + 2 ml of DMEM in the bottom of the dish. The lids were then carefully inverted so cells remained suspended and were allowed to aggregate by gravity. The cultures were maintained at 37°C and 5% (mVSMCs) or 10% (hVSMCs) CO_2. VSMC spheroids formed after 24 to 48 hours of incubation. Images were taken at 10X magnification using an upright Olympus BH-2 microscope equipped with a digital camera (AmScope) to assess spheroid formation.

Protein extraction and immunoblotting

Total cell lysates were prepared from hVSMC and mVSMC spheroids. Spheroids were collected in 1.7 mL Eppendorf tubes, centrifuged, and extracted in 1X TNE lysis buffer [50 mM Tris-HCl (pH 8.0), 250 mM NaCl, 2 mM EDTA, 1% Nonidet P-40, plus protease and phosphatase inhibitor cocktail composed of a proprietary mix of AEBSF, Aprotinin, Bestatin, E64, Leupeptin, and Pepstatin A to promote broad spectrum protection against endogenous proteases]. Equal

amounts of extracted protein were mixed with 5x sample buffer [250 mM Tris-HCl (pH 6.8), 10% SDS, 50% glycerol, 0.02% bromophenol blue, 10 mM 2-mercaptoethanol], denatured by boiling samples at 100°C, subjected to 8% sodium dodecyl sulfate polyacrylamide gel electrophoresis (SDS-PAGE) and transferred to a polyvinylidene difluoride (PVDF) membrane. The PVDF membranes were blocked with either 5% BSA or 5% milk in 1X TBST (Tris-buffered saline, 0.1% Tween 20) for 1 hour and probed with primary antibodies to: FAK (Invitrogen, 39-6500), phospho-FAK (Invitrogen, 44-624G), N-cadherin (Proteintech, 22018-I-AP), and GAPDH (Proteintech, 60004-I-Ig). After overnight incubation at 4°C, the PVDF membranes were washed with 1X TBST and probed with horseradish peroxidase (HRP) conjugated secondary antibodies (Bio-Rad) for 2 to 5 min. Immunoblot signals were detected using chemiluminescence (Bio-Rad).

VGG16-U-Net based semantic segmentation

The U-Net based image segmentation was designed to automatically segment the spheroid images. The morphological features of the object of interest are extracted. The framework could be divided into two parts: an encoder that extracts image features and a decoder that identifies the edge location using the extracted features. In order to use a limited number of training images, the pre-trained VGG-16 model is reused in the encoder and extracts features in a different level. The second difference from U-net is that in the decoder, a simpler and asymmetric framework is incorporated to detect the edge, which substantially reduces the model complexity. In comparison to U-net, the VGG16-U-net includes fewer trainable parameters, which will use much fewer training sets. Training the model with very limited images and evaluating the performance on the entire dataset to identify the challenging regions were possible with higher precision. The model can be retrained iteratively until a satisfied performance is achieved.

The working chain of operation starts with the manual segmentation of boundaries. This is followed by training the algorithm to identify spheroid boundaries by learning boundary parameters.

i. ***Manual segmentation:*** A set of twenty VSMC spheroids from each of the DMSO (vehicle control) and drug-treated groups (for FAK, Rac, Rho and Cdc42) were randomly selected and spheroid boundaries were drawn using the Pixel Annotation Tool software (https://github.com/abreheret/PixelAnnotationTool). The boundary of each individual spheroid was traced and the resultant images were used as raw images.

ii. ***Binary image and training data generation:*** Images of the hand-drawn boundaries were used to generate binary images. The hand-drawn masks were used to train the algorithm. The masks are used as a training data set from which the algorithm learns to identify the boundary of the spheroid. The generated masks are then overlapped with raw images to visualize the learning efficiency of the algorithm. To validate the performance of the algorithm, the dice co-efficient and training loss was plotted.

iii. ***Feature extraction and feature vector generation:*** The binary images were processed for extracting the morphological features. The morphological features were used to graphically represent the response of the spheroid to FAK, Rac Rho, and Cdc42 inhibitors and DMSO (vehicle control) treatment. Morphological features were extracted from binary images. The morphological features extracted are listed in section 3.4.5. Once the features were generated, the feature vector matrix was generated and global z normalization was performed on the data. Z-score normalization on each experiment was useful to remove some batch-effects and global z-score normalization was used before PCA always to unify the variance. The data points in the feature vector matrix was normalized to the mean of the same experimental groups and group data set values[45].

iv. ***Dimensionality reduction and Data representation:*** The feature vectors extracted from

the spheroids were plotted in Umap plot. Umap is a form of dimensionality reduction scatter plot that uses k-mean values and is fast and efficient to perform clustering analysis[30].

v. ***Clustering analysis using k-means clustering:*** The feature vectors generated from spheroid images were analyzed for the presence of clusters to identify the presence of morphological subpopulations arising due to drug responses. The k-means clustering analysis identifies k number of centroids (from each group of points) and then allocates every data point to the nearest cluster while keeping the centroids as small as possible. The k-means clustering is a type of unsupervised learning, which is used when there are unlabeled data (i.e., data without defined categories or groups). Following the clustering analysis, the feature vector matrix was matched to the image data set to categorize the images based on the clustering results. This was performed to identify the morphology of the spheroids that are present in a single cluster. The clustering analysis was performed in two steps (Fig. 2): Coarse Clustering (step 1) and Fine-tuning Clustering (step 2).

v-i ***Coarse Clustering (Step 1):*** Four morphological features relating to the roundness of the spheroids were used for clustering the spheroids. The four features selected were Number of Colonies, Circularity (The circularity value is computed as (4*Area*pi)/ (Perimeter2). For a perfect circle, the circularity value is 1.), Extent (the spheroid colony with the largest area), Solidity (Proportion of the pixels in the convex polygon that are also in the region) and Eccentricity (An ellipse whose eccentricity is 0 is a circle, while an ellipse whose eccentricity is 1) (Fig. 2). Based on the distribution of spheroids in these clusters, a proportionality plot (see Fig. 10B) was drawn with cluster number in X-axis and the proportion of the total spheroid in each DMSO or drug treatment groups. The images of spheroids were identified by matching the feature

vector of a data point in the cluster to the spheroid from which it was extracted. The resulting clusters were expected to show clusters of spheroid images with round morphology and clusters with disrupted morphologies.

v-ii ***Fine-Tuning Clustering (Step 2):*** Resultant clusters from coarse clustering were further analyzed. Clusters containing non-circular spheroids (based on the number of colonies and circularity) were selected and more features were explored for clustering to best fine-tune said clusters (Fig. 2). Additional morphological features were extracted from the non-spherical spheroid clusters. These morphological features were more focused on exploring morphology various disruption patterns of the spheroid. The morphological features extracted includes *Area* (area of all the pixels in the largest external contour), *Major axis length* (length in pixels of the major axis of the ellipse that has same normalized second central moments as the region), *Minor axis length* (Length in pixels of the minor axis of the ellipse that has same normalized second central moments as the region), *Eccentricity*, *Solidity*, *Extent* (ratio of pixels in the region to pixels in the total bounding box, returned as a scalar), *Perimeter* (distance around the boundary of the region returned as a scalar), *Convex area* (number of pixels in the bounding box of the region), *Circularity*, *Aspect ratio*, *Actual area*, *Actual equivalent diameter* (diameter of a sphere with the same volume as the region), *Actual circularity*, and *Number of holes* (number of internal contours).

Statistical analysis

Data are presented as mean + standard deviation (SD) of the indicated number of independent experiments. Data were analyzed using student t-test. Results with p-values lower than 0.05 (*), 0.01 (**), or 0.001 (***) were considered to be statistically significant.

REFERENCES

1 Pizzolato, R. & Romero, J. M. in *Handbook of Clinical Neurology* Vol. 135 (eds Joseph C. Masdeu & R. Gilberto González) 165-191 (Elsevier, 2016).

2 Chen, C.-H. & Kirtane, A. J. in *The Interventional Cardiac Catheterization Handbook (Fourth Edition)* (eds Morton J. Kern, Paul Sorajja, & Michael J. Lim) 179-199 (Elsevier, 2018).

3 Fattori, R. & Piva, T. Drug-eluting stents in vascular intervention. *The Lancet* **361**, 247-249, doi:https://doi.org/10.1016/S0140-6736(03)12275-1 (2003).

4 Stadler, M. *et al.* Exclusion from spheroid formation identifies loss of essential cell-cell adhesion molecules in colon cancer cells. *Sci Rep* **8**, doi:10.1038/s41598-018-19384-0 (2018).

5 Lin, R.-Z., Chou, L.-F., Chien, C.-C. & Chang, H.-Y. Dynamic analysis of hepatoma spheroid formation: Roles of E-cadherin and β1-integrin. *Cell and tissue research* **324**, 411-422, doi:10.1007/s00441-005-0148-2 (2006).

6 Shimazui, T. *et al.* Role of complex cadherins in cell-cell adhesion evaluated by spheroid formation in renal cell carcinoma cell lines. *Oncology reports* **11**, 357-360 (2004).

7 Strauss, B. H. *et al.* Extracellular matrix remodeling after balloon angioplasty injury in a rabbit model of restenosis. *Circulation research* **75**, 650-658, doi:10.1161/01.res.75.4.650 (1994).

8 Calvete, J. J. Structures of integrin domains and concerted conformational changes in the bidirectional signaling mechanism of alphaIIbbeta3. *Experimental biology and medicine (Maywood, N.J.)* **229**, 732-744, doi:10.1177/153537020422900805 (2004).

9 Duband, J. L., Rocher, S., Chen, W. T., Yamada, K. M. & Thiery, J. P. Cell adhesion and migration in the early vertebrate embryo: location and possible role of the putative fibronectin receptor complex. *The Journal of cell biology* **102**, 160-178, doi:10.1083/jcb.102.1.160 (1986).

10 Jones, M., Sabatini, P. J. B., Lee, F. S. H., Bendeck, M. P. & Langille, B. L. N-Cadherin Upregulation and Function in Response of Smooth Muscle Cells to Arterial Injury. *Arteriosclerosis, Thrombosis, and Vascular Biology* **22**, 1972-1977, doi:doi:10.1161/01.ATV.0000036416.14084.5A (2002).

11 Dwivedi, A., Sala-Newby, G. B. & George, S. J. Regulation of cell–matrix contacts and β-catenin signaling in VSMC by integrin-linked kinase: implications for intimal thickening. *Basic Research in Cardiology* **103**, 244-256, doi:10.1007/s00395-007-0693-9 (2008).

12 Mui, K. L. *et al.* N-cadherin induction by ECM stiffness and FAK overrides the spreading requirement for proliferation of vascular smooth muscle cells. *Cell reports* **10**, 1477-1486 (2015).

13 Blindt, R. *et al.* Downregulation of N-cadherin in the neointima stimulates migration of smooth muscle cells by RhoA deactivation. *Cardiovascular research* **62**, 212-222 (2004).

14 Riedl, J. *et al.* Lifeact: a versatile marker to visualize F-actin. *Nat Meth* **5**, 605-607, doi:http://www.nature.com/nmeth/journal/v5/n7/suppinfo/nmeth.1220_S1.html (2008).

15 Li, C. *et al.* RhoA determines lineage fate of mesenchymal stem cells by modulating CTGF–VEGF complex in extracellular matrix. *Nature Communications* **7**, 11455, doi:10.1038/ncomms11455 (2016).

16 Webb, D. J., Parsons, J. T. & Horwitz, A. F. J. N. c. b. Adhesion assembly, disassembly and turnover in migrating cells–over and over and over again. **4**, E97 (2002).

17 Tang, D. D. & Gunst, S. J. The Small GTPase Cdc42 Regulates Actin Polymerization and Tension Development during Contractile Stimulation of Smooth Muscle. **279**, 51722-51728, doi:10.1074/jbc.M408351200 (2004).

18 Parri, M. & Chiarugi, P. Rac and Rho GTPases in cancer cell motility control. *Cell Commun Signal* **8**, 23-23, doi:10.1186/1478-811X-8-23 (2010).

19 Takaishi, K., Sasaki, T., Kotani, H., Nishioka, H. & Takai, Y. Regulation of cell-cell adhesion by rac and rho small G proteins in MDCK cells. *The Journal of cell biology* **139**, 1047-1059, doi:10.1083/jcb.139.4.1047 (1997).
20 Mabuchi, I. *et al.* A rho-like protein is involved in the organisation of the contractile ring in dividing sand dollar eggs. *Zygote* **1**, 325-331, doi:10.1017/S0967199400001659 (1993).
21 Çiçek, Ö., Abdulkadir, A., Lienkamp, S. S., Brox, T. & Ronneberger, O. in *International conference on medical image computing and computer-assisted intervention.* 424-432 (Springer).
22 Simonyan, K. & Zisserman, A. J. a. p. a. Very deep convolutional networks for large-scale image recognition. (2014).
23 Wang, C. *et al.* Deep learning pipeline for cell edge segmentation of time-lapse live cell images. 191858, doi:10.1101/191858 %J bioRxiv (2019).
24 Braren, R. *et al.* Endothelial FAK is essential for vascular network stability, cell survival, and lamellipodial formation. **172**, 151-162, doi:10.1083/jcb.200506184 %J The Journal of Cell Biology (2006).
25 Cheng, Z. *et al.* Focal Adhesion Kinase Regulates Smooth Muscle Cell Recruitment to the Developing Vasculature. **31**, 2193-2202, doi:doi:10.1161/ATVBAHA.111.232231 (2011).
26 Li, J.-J., Han, M., Wen, J.-K. & Li, A.-Y. Osteopontin stimulates vascular smooth muscle cell migration by inducing FAK phosphorylation and ILK dephosphorylation. *Biochemical and Biophysical Research Communications* **356**, 13-19, doi:https://doi.org/10.1016/j.bbrc.2007.02.092 (2007).
27 Laszlo, V. *et al.* The FAK inhibitor BI 853520 inhibits spheroid formation and orthotopic tumor growth in malignant pleural mesothelioma. *Journal of Molecular Medicine* **97**, 231-242, doi:10.1007/s00109-018-1725-7 (2019).
28 Braga, V. M., Machesky, L. M., Hall, A. & Hotchin, N. A. The small GTPases Rho and Rac are required for the establishment of cadherin-dependent cell-cell contacts. *The Journal of cell biology* **137**, 1421-1431, doi:10.1083/jcb.137.6.1421 (1997).
29 Braga, V. M. M., Betson, M., Li, X. & Lamarche-Vane, N. Activation of the Small GTPase Rac Is Sufficient to Disrupt Cadherin-dependent Cell-Cell Adhesion in Normal Human Keratinocytes. *Molecular Biology of the Cell* **11**, 3703-3721, doi:10.1091/mbc.11.11.3703 (2000).
30 Becht, E. *et al.* Dimensionality reduction for visualizing single-cell data using UMAP. *Nature Biotechnology* **37**, 38-44, doi:10.1038/nbt.4314 (2019).
31 Vento-Tormo, R. *et al.* Single-cell reconstruction of the early maternal–fetal interface in humans. *Nature* **563**, doi:10.1038/s41586-018-0698-6 (2018).
32 Sommer, F., Fouss, F. & Saerens, M. in *International Conference on Artificial Neural Networks.* 423-433 (Springer).
33 Liu, S.-L. *et al.* Matrix metalloproteinase-12 is an essential mediator of acute and chronic arterial stiffening. *Sci Rep* **5**, 17189-17189, doi:10.1038/srep17189 (2015).
34 Badea, M. A. *et al.* Influence of Matrigel on Single- and Multiple-Spheroid Cultures in Breast Cancer Research. *SLAS discovery : advancing life sciences R & D* **24**, 563-578, doi:10.1177/2472555219834698 (2019).
35 Yano, H. *et al.* Roles played by a subset of integrin signaling molecules in cadherin-based cell–cell adhesion. *The Journal of cell biology* **166**, 283-295, doi:10.1083/jcb.200312013 (2004).
36 Gao, L., McBeath, R. & Chen, C. S. J. S. c. Stem cell shape regulates a chondrogenic versus myogenic fate through Rac1 and N-cadherin. **28**, 564-572 (2010).
37 Feil, S. *et al.* Transdifferentiation of vascular smooth muscle cells to macrophage-like cells during atherogenesis. *Circulation research* **115**, 662-667, doi:10.1161/circresaha.115.304634 (2014).
38 Nobes, C. D. & Hall, A. Rho, Rac, and Cdc42 GTPases regulate the assembly of

multimolecular focal complexes associated with actin stress fibers, lamellipodia, and filopodia. *Cell* **81**, 53-62, doi:10.1016/0092-8674(95)90370-4 (1995).

39 Zanoni, M. *et al.* 3D tumor spheroid models for in vitro therapeutic screening: a systematic approach to enhance the biological relevance of data obtained. *Sci Rep* **6**, 19103, doi:10.1038/srep19103 https://www.nature.com/articles/srep19103#supplementary-information (2016).

40 Chappell, J. *et al.* Extensive proliferation of a subset of differentiated, yet plastic, medial vascular smooth muscle cells contributes to neointimal formation in mouse injury and atherosclerosis models. **119**, 1313-1323 (2016).

41 Laurent, J. *et al.* Multicellular tumor spheroid models to explore cell cycle checkpoints in 3D. *BMC Cancer* **13**, 73-73, doi:10.1186/1471-2407-13-73 (2013).

42 Bae, Y. H. *et al.* A FAK-Cas-Rac-lamellipodin signaling module transduces extracellular matrix stiffness into mechanosensitive cell cycling. *Science signaling* **7**, ra57, doi:10.1126/scisignal.2004838 (2014).

43 Hsu, B. Y., Bae, Y. H., Mui, K. L., Liu, S. L. & Assoian, R. K. Apolipoprotein E3 Inhibits Rho to Regulate the Mechanosensitive Expression of Cox2. *PLoS One* **10**, e0128974, doi:10.1371/journal.pone.0128974 (2015).

44 Foty, R. A simple hanging drop cell culture protocol for generation of 3D spheroids. *Journal of visualized experiments : JoVE*, 2720, doi:10.3791/2720 (2011).

45 Cao, X. H., Stojkovic, I. & Obradovic, Z. A robust data scaling algorithm to improve classification accuracies in biomedical data. *BMC Bioinformatics* **17**, 359-359, doi:10.1186/s12859-016-1236-x (2016).

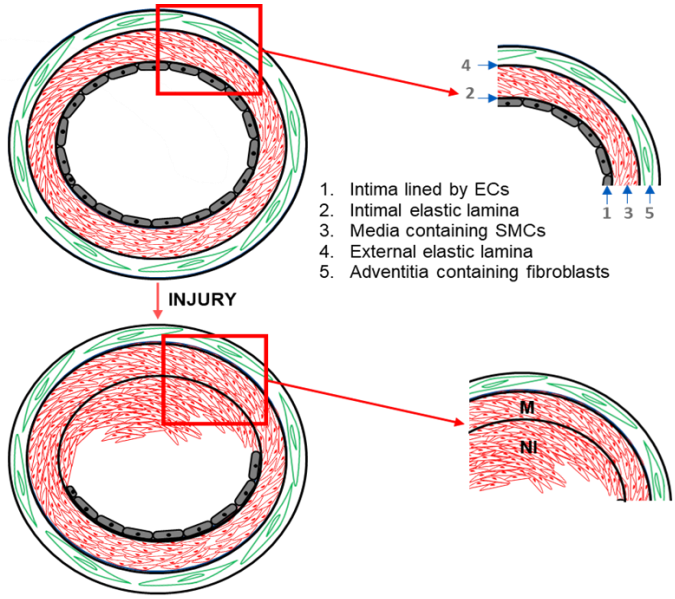

Figure 1: Neointima formation after vascular injury: **(A)** Injury to the intimal layer (layer 1) of the healthy vessel results in the loss of endothelial cells. VSMCs from the media layer (layer 3) de-differentiates, migrates and proliferates to the intima forming the neointima (NI). **(B)** The NI can reduce blood flow by partially occluding the vessel.

Figure 2: Two-level framework for k-means clustering: Spheroid images were segmented by VGG16-U-Net semantic segmentation and feature vectors were extracted for additional clustering analysis. Two level framework was used to analyze the presence of morphological subpopulations of spheroids. Level 1 clustering analysis is coarse clustering and is based on roundness of the spheroids. Level 2 clustering is fine-tune clustering and the non-round spheroids from coarse clustering were clustered based on the morphology of disruption.

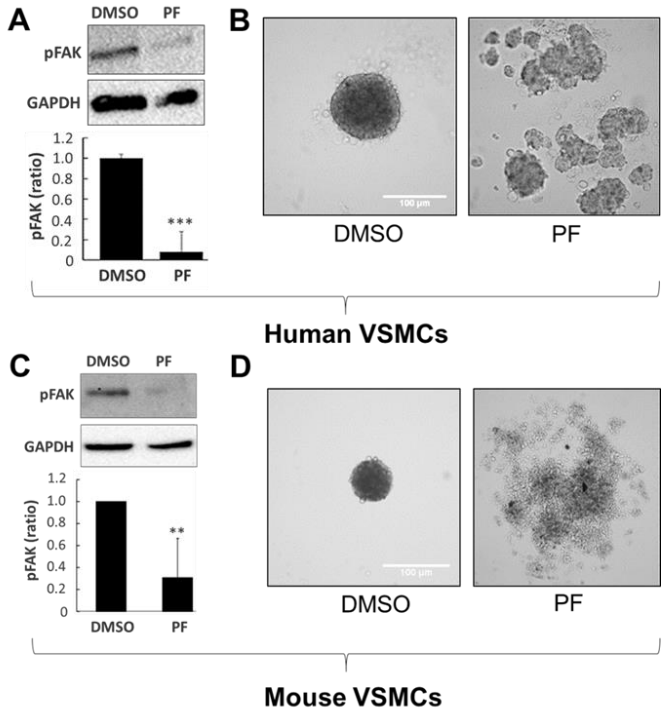

Figure 3: FAK is essential for spheroid formation. Human VSMC (**5A-5B**) and mouse VSMC (**5C-5D**) spheroids were made using a hanging drop technique with 2000 cells per droplet in the presence of either 10 µM PF573228 (PF) or DMSO (vehicle control) in high glucose DMEM containing 10% serum. Total cell lysates were immunoblotted (**5A** and **5C**) for phosphorylated FAK at Tyr397 (pFAK) and GAPDH. Cultures were imaged after 24 hours of incubation using an upright microscope (**5B** and **5D**). *n*=4 (A), *n*=7 (B), *n*=4 (C), and *n*=12 (D) biological replicates were used. ***p<0.01 or p***<0.001.*

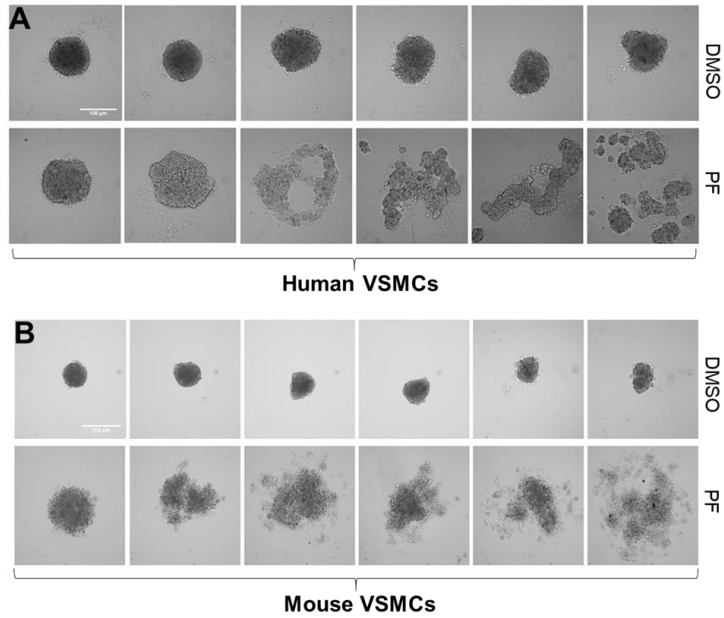

Figure 4: FAK inhibition shows heterogeneous patterns of disruption in VSMC spheroids. VSMCs spheroids were made in the presence of either 10 µM PF573228 (PF) or DMSO (vehicle control) in high glucose DMEM. Cultures were imaged after 24 hours of incubation using an upright microscope.

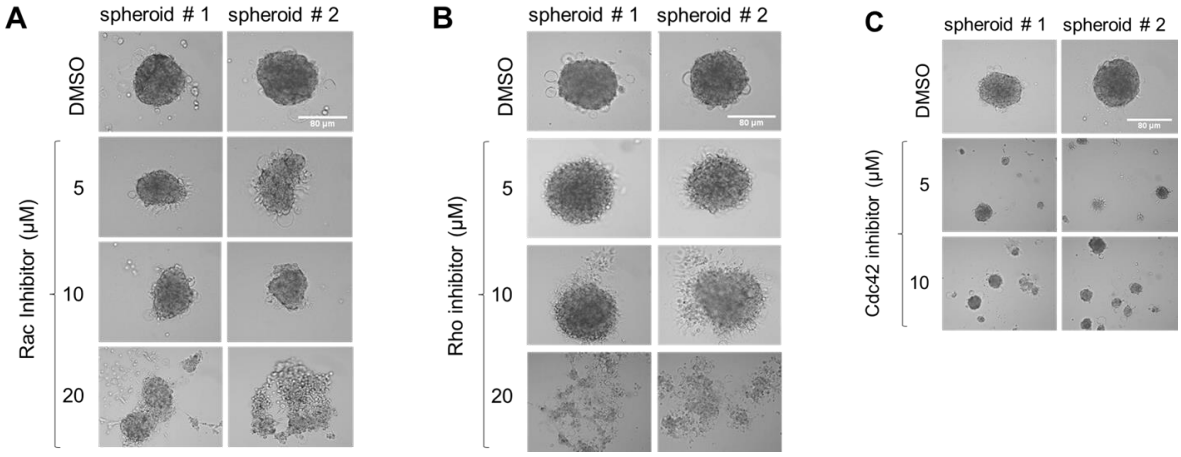

Figure 5: Rac, Rho, and Cdc42 are essential for hVSMC spheroid formation. hVSMCs treated with inhibitors of 5-20 μM EHT1864 **(A**, Rac inhibitor**)**, 5-20 μM Rhosin **(B**, Rho inhibitor**)**, or 5-10 μM ML141 **(C**, Cdc42 inhibitor**)**, or vehicle control (DMSO) were used to generate 3D spheroids. Bright field images of the resultant spheroids were acquired using an upright microscope.

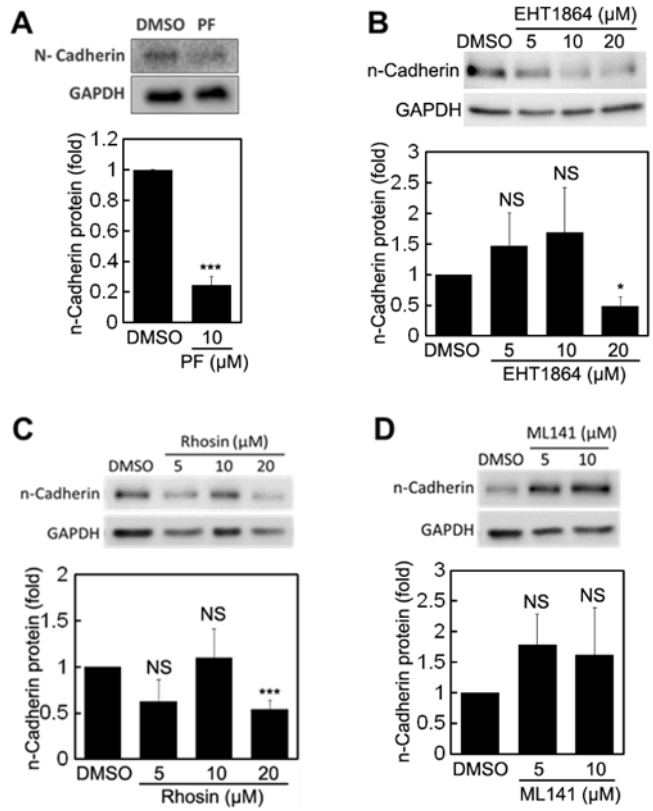

Figure 6: FAK, Rac and Rho inhibition disrupts VSMC spheroid formation through N-cadherin. hVSMCs treated with 10μM PF573228 **(A)**, 5-20 μM EHT1864 **(B)**, 5-20 μM Rhosin **(C)**, 5-10 μM ML141 **(D)**, or DMSO were used to generate spheroids. Total cell lysates were immunoblotted for N-cadherin and GAPDH. *n*=5 biological replicates were used. *p*<0.05 or p***<0.0001.*

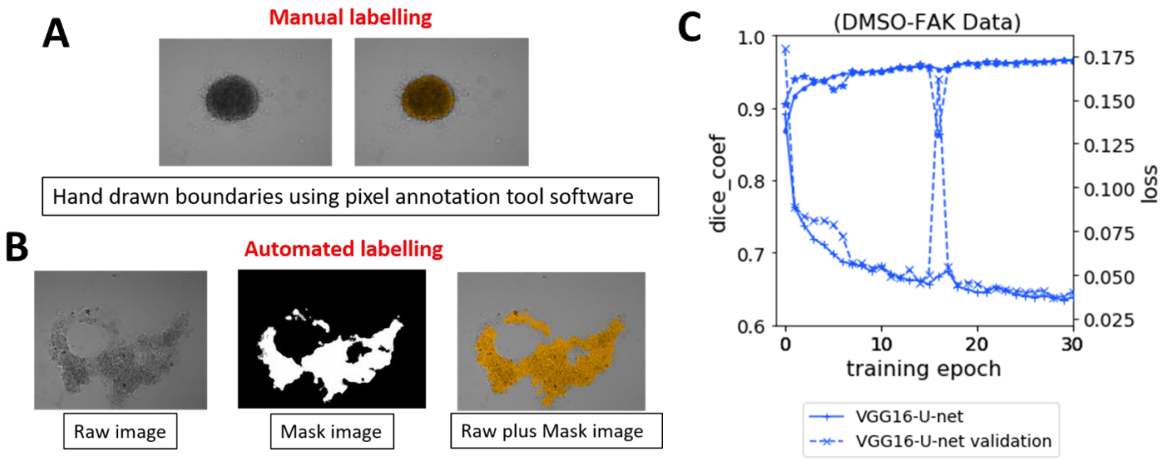

Figure 7: VGG16-U-Net based image segmentation. Pre-processing and generating masks from the bright field images of the spheroids. **(A)** Pixel annotation tool software was used to hand-draw outlines of spheroids. **(B)** The image boundary was identified by the algorithm, converted to binary images, and overlapped with raw images to evaluate the efficiency of the algorithm. **(C)** The training and validation performance was plotted together on loss function and dice-coefficient (dice_coef). The training performance kept increasing during the iterations (epoch).

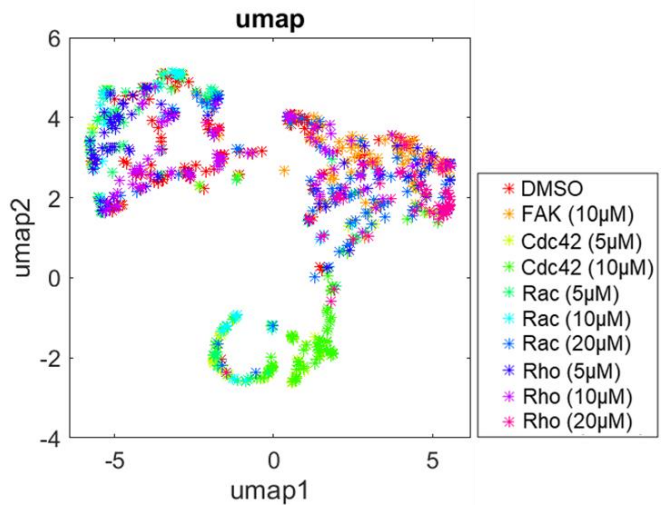

Figure 8: Four feature Umap plot shows presence of morphological heterogeneity in response to drug treatments: Four morphological features extracted from hVSMC spheroid images were plotted as Umap plot. Different colored '*'s are used to represent the various drug treatments; FAK (PF573228 treated spheroids), Rac (EHT 1864 treated spheroids), Rho (Rhosin treated spheroids) and Cdc42 (ML141 treated spheroids).

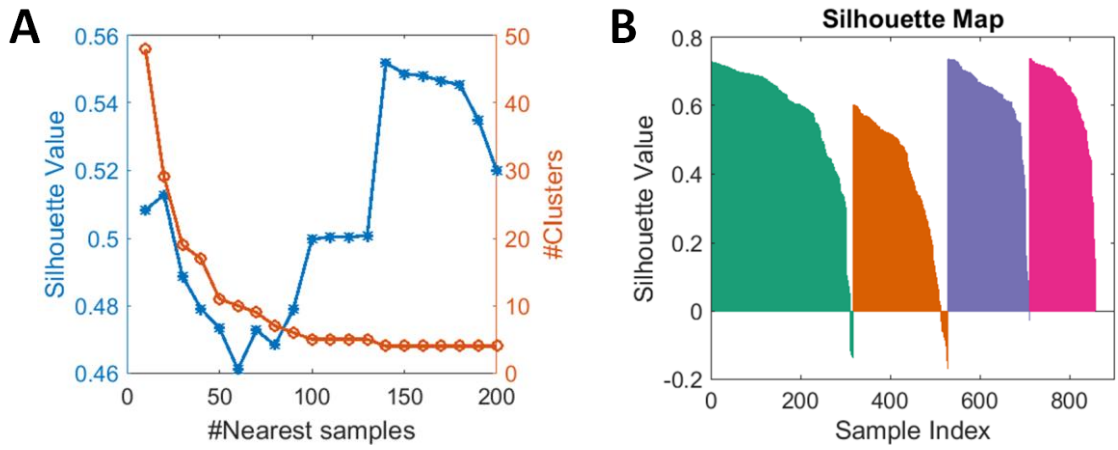

Figure 9: Cluster evaluation for coarse clustering displays presence of 4 distinct morphological clusters: (A) #nearest samples between 2 and 200 were evaluated and the silhouette values were plotted. A cluster number of 4 was selected. **(B)** A silhouette map for 4 clusters showed highest positive silhouette values and less overlap between clusters.

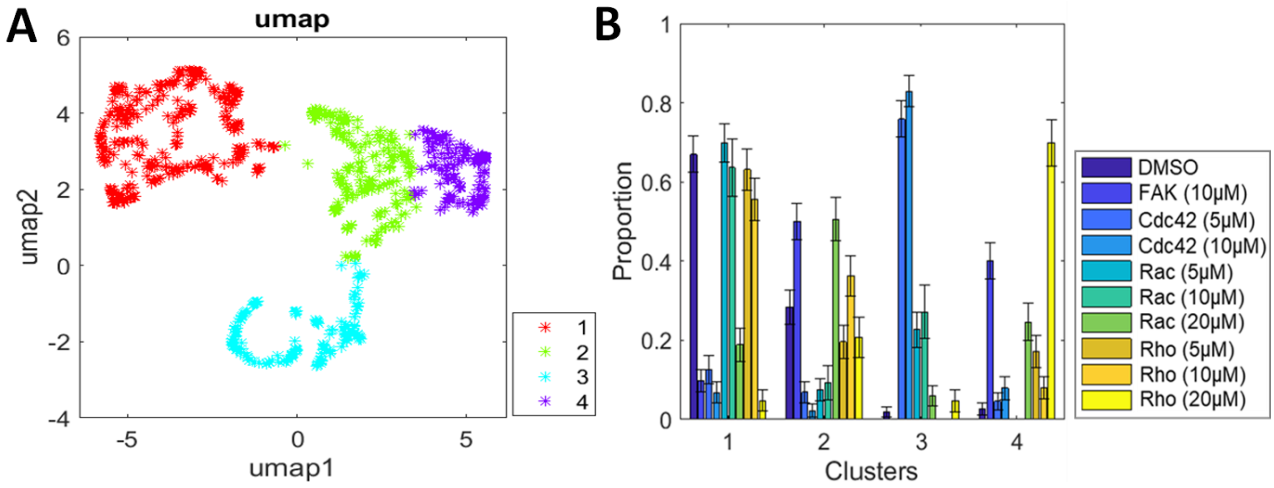

Figure 10: Coarse clustering using k-means clustering analysis identifies 4 morphologically distinct clusters in responses to inhibitors of FAK and small G1 proteins on hVSMC spheroid formation: (A) 4 morphological clusters plotted on the Umap were observed based on the "roundness of the spheroid". Different colored '*'s are used to represent the various morphological clusters with treatments**. (B)** A proportionality plot was graphed to identify the distribution of spheroids in each morphological cluster with treatments.

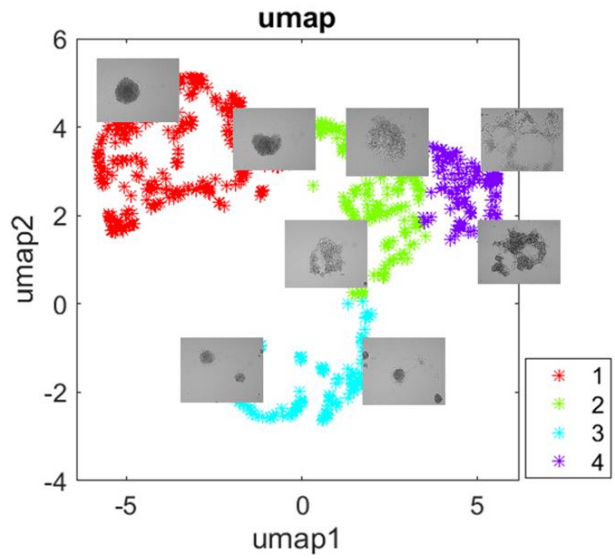

Figure 11: Morphological clusters showing spheroid images in each clusters: The most representative images were inserted into each cluster (2 images per cluster) in the Umap used in figure 12. Clusters 1 and 3 showed spheroids with circular morphology and the spheroids in clusters 2 and 4 showed disrupted/dispersed or irregular morphologies.

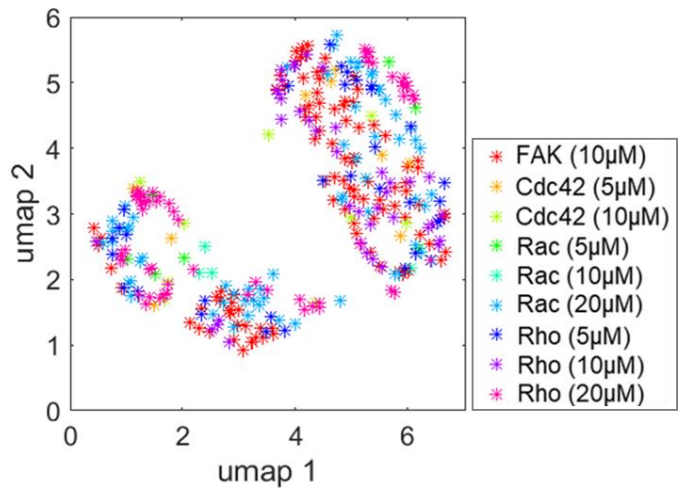

Figure 12: Fine tuning clustering analysis (step 2) shows the presence of 4 distinct clusters with disrupted morphology. Fifteen morphological features extracted from hVSMC spheroid images from clusters 2 and 4 after coarse clustering were graphed as Umap plot. Different colored '*'s are used to represent the various drug treatments.

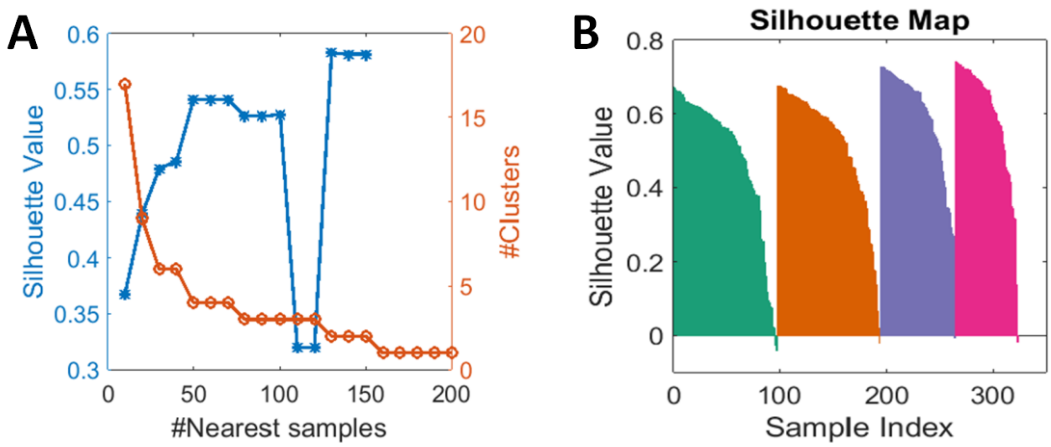

Figure 13: Fine-tune k-means Cluster evaluation shows presence of 4 distinct morphological clusters: (A) #nearest sample between 2 and 200 were evaluated and the silhouette values were plotted. Cluster number of 4 was selected. **(B)** Silhouette map for 4 clusters show highest positive silhouette value and less overlap between clusters.

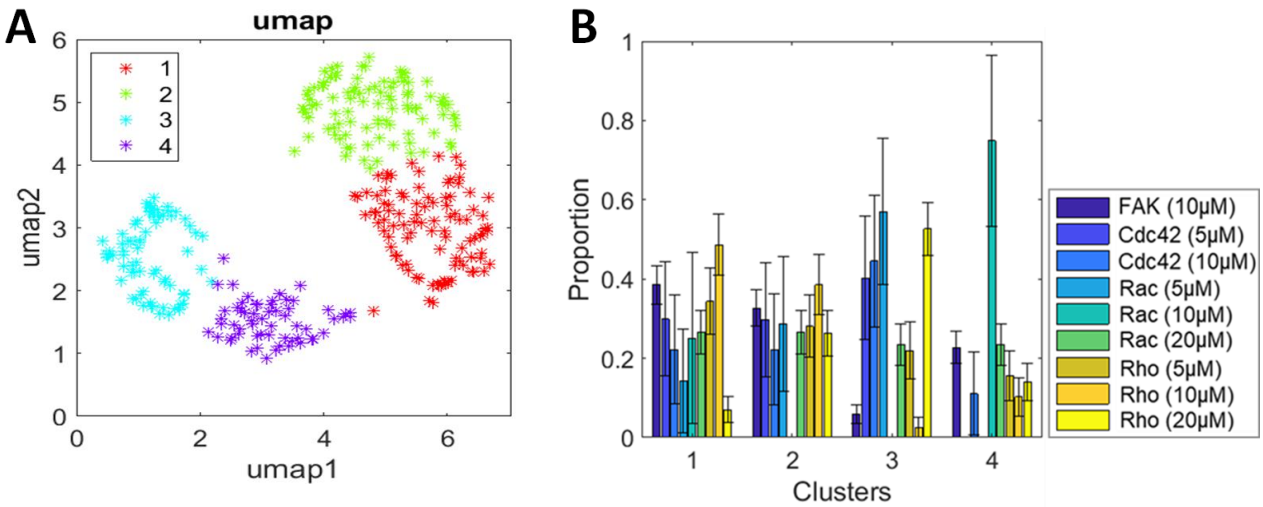

Figure 14: Fine tune k-means clustering reveals 4 morphological clusters in responses to inhibitory drugs on hVSMC spheroid formation: (A) Four morphological clusters were observed based on the disrupted spheroid from cluster 2 and 4 obtained from coarse clusters. Different colored '*'s are used to represent the various morphological clusters. **(B)** Proportionality plots were plotted to identify the distribution of spheroids in each morphological cluster.

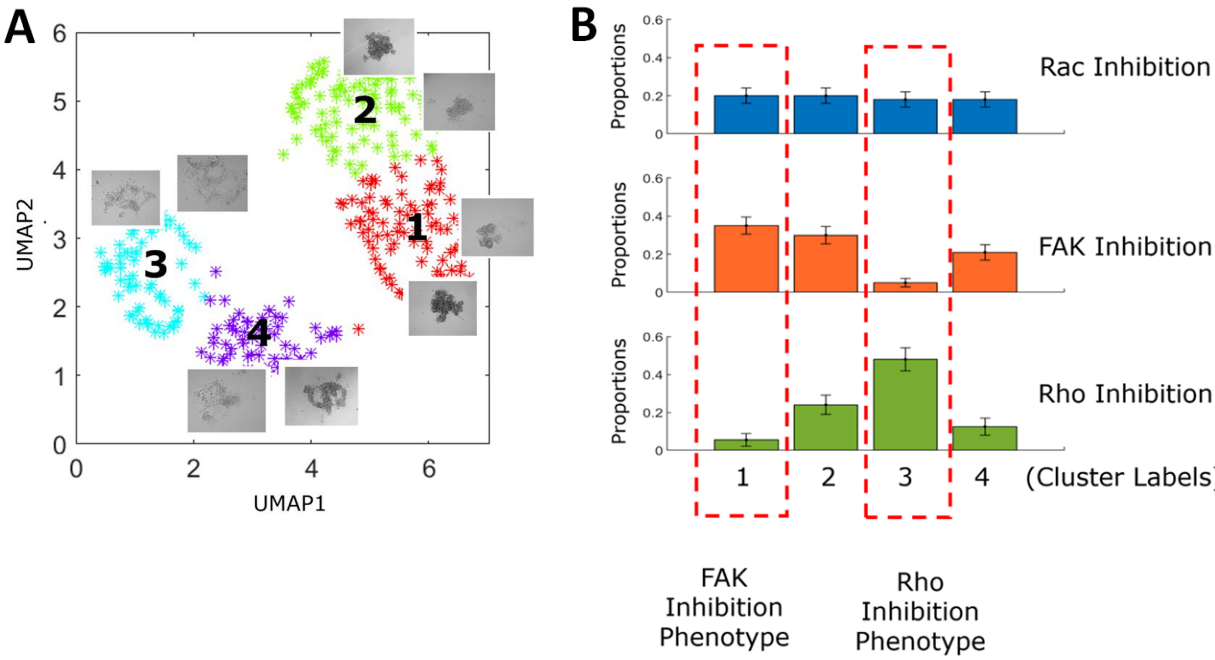

Figure 15: Fine-tune k-means clustering reveals 4 morphological clusters in responses to inhibitory drugs on hVSMC spheroid formation: (A) Four morphological clusters were observed based on the various disruption patterns of spheroids. The morphology of spheroids in each cluster was mapped. **(B)** The proportionality plot shows the distribution of spheroid morphologies corresponding to the drug treatment.

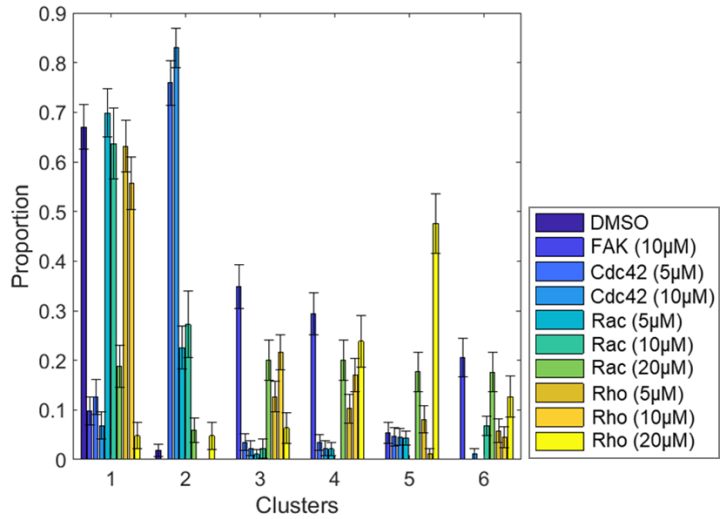

Figure 16: Coarse and Fine clustering analyses define 6 morphological clusters in responses to inhibitors of FAK, Rac, Rho, or Cdc42, or DMSO on hVSMC spheroid formation: Proportionality plots were plotted by combining coarse and fine tuning clustering to identify the distribution of all the spheroids in each morphological cluster. Clusters 1 and 2 are spheroids with circular morphology observed in clusters 1 and 3 after coarse clustering. The spheroids in cluster 2 through 6 showed disrupted or irregular morphologies observed after fine tuning clustering.